Mechanism of Taq DNA Polymerase Inhibition by Fullerene Derivatives: Insight from Computer Simulations

ARTICLE *in* THE JOURNAL OF PHYSICAL CHEMISTRY B · AUGUST 2012

Impact Factor: 3.3 · DOI: 10.1021/jp3046577 · Source: PubMed

3 AUTHORS, INCLUDING:

Praveen Nedumpully Govindan
Clemson University
19 PUBLICATIONS **106** CITATIONS
SEE PROFILE

Luca Monticelli
French National Centre for Scientific Research
80 PUBLICATIONS **2,674** CITATIONS
SEE PROFILE

THE JOURNAL OF PHYSICAL CHEMISTRY B

Article

pubs.acs.org/JPCB

Mechanism of *Taq* DNA Polymerase Inhibition by Fullerene Derivatives: Insight from Computer Simulations

Praveen Nedumpully Govindan,[†] Luca Monticelli,[‡,∥,§] and Emppu Salonen*[,†]

[†]Department of Applied Physics, Aalto University, P.O. Box 11100, FI-00076 AALTO, Finland

[‡]INSERM, UMR-S665, Paris, France

[∥]Université Paris Diderot, Sorbonne Paris Cité, UMR-S 665, Paris, France

[§]Institut National de la Transfusion Sanguine (INTS), Paris, France

Supporting Information

ABSTRACT: Experiments have shown that two water-soluble fullerene C_{60} derivatives, fullerenol and fullerene trimalonic acid, inhibit duplication of DNA via polymerase chain reaction (PCR). It has further been shown that the target of this inhibition is the DNA polymerase protein routinely used in PCR. We have used a combination of molecular docking and molecular dynamics simulations to study the possible DNA polymerase inhibition mechanisms in atomistic detail. The simulations show structural changes in the tip and two alpha helices of a subdomain, crucial for the polymerase activity, upon fullerene derivative binding. Such tertiary structure changes could prevent the binding of DNA to the protein, causing the inhibition of the PCR process. These findings are in agreement with experimental studies, which have shown that the inhibition is not competitive. The proposed mechanism of inhibition would be common for all DNA polymerase proteins, providing new possibilities in antiviral applications of fullerene derivatives.

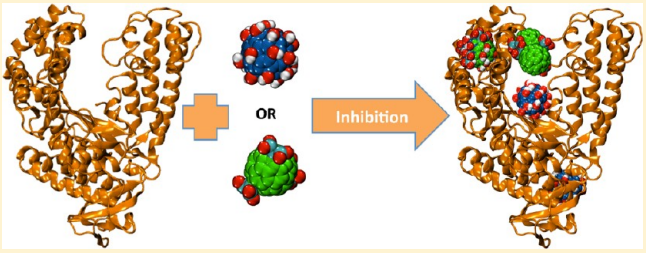

INTRODUCTION

Since the development of methods to produce fullerenes on a commercial scale and the synthesis of the first water-soluble fullerene derivatives in the early 1990s, there has been great interest in exploring their possible biomedical applications.[1−5] The motivation for such studies results from a combination of interesting physicochemical properties of fullerenes. They are small (of the order of 1 nm in diameter), and the enclosed shape of fullerenes makes it possible to modify their electronic properties by encapsulation of metal atoms (endofullerenes).[6] Fullerenes have also intriguing photodynamic properties[7,8] and they are good electron acceptors.[9] Advances in fullerene chemistry have resulted in techniques to attach functional groups on fullerene surfaces in a controlled fashion.[9−11] In addition to rendering fullerenes water-soluble, chemical functionalization provides ways to modify their properties for supramolecular assembly.[11−13]

The potential of fullerenes for biomedical applications is attested, e.g., by studies employing fullerenes in MRI imaging as contrast agents,[14,15] in gene[16,17] and drug delivery,[18] quenching of reactive oxygen species (ROS)[19] and photocleaving of DNA.[20−22] Much work has been devoted to testing inhibition of enzymatic function by fullerene derivatives, such as in the cases of HIV-1 protease (HIV1P),[23] HIV reverse transcriptase (HIV-RT), and hepatitis C virus RNA-dependent RNA polymerase (HCV-RP).[24] All these enzymes are crucial for viral replication and survival, and functionalized fullerenes are consequently viewed as attractive potential antiviral agents.[1−5]

Polymerase chain reaction (PCR) is a standard method for amplification of DNA in vitro. The method is based on a succession of heating/cooling cycles: (1) denaturation of DNA double strands to be amplified into single-stranded templates; (2) annealing of short, complementing DNA strands (primers) to the single-stranded templates; and (3) synthesis of new DNA strands by enzymes called DNA polymerases via recognition of the primer-template double strands. Due to its exceptional stability at high temperatures, the most commonly used DNA polymerase in PCR at present is *taq* DNA polymerase (*taq* pol for short), originating from the thermophilic bacterium *Thermus aquaticus*.[25]

Recently, Meng et al. demonstrated the inhibition of PCR by both polyhydroxylated fullerenes (fullerenols) $C_{60}(OH)_x$ and trimalonic acid C_{60} derivatives.[26] They showed that increasing the concentration of the DNA primers had little effect on the fullerene derivative-induced inhibition. Increasing the concentration of *taq* pol, on the other hand, could reverse the effect of the fullerene derivatives, and it was concluded that the enzyme was the target in the PCR inhibition. These results were later corroborated by Shang et al. using real-time PCR.[27] In addition

Received: May 14, 2012
Revised: August 15, 2012
Published: August 16, 2012

to ascertaining the inhibition of PCR by the fullerenol $C_{60}(OH)_{20}$, monitoring the DNA amplification efficiency showed a clear delay for fullerenol concentrations at which the inhibition was observed.

Taq pol has three domains: a 5′ nuclease domain, a polymerase domain, which catalyzes the polymerization reaction, and an inactive 3′-5′ exonuclease domain.[28] The polymerase domain resembles a right-hand with three subdomains called "thumb", "fingers", and "palm".[29] The fidelity of the protein can be improved by cleaving the 5′ nuclease domain, and the resulting large fragment is called the "Klentaq fragment"[30] (see Figure 1). For catalyzing the polymerization reaction, *taq* pol binds to a single-stranded DNA with a bound primer and aligns it properly.[31] During this process, a large conformational change occurs in the thumb subdomain. Provided that the right type of a deoxy-nucleoside triphosphate (dNTP) binds to the protein at the O-helix of the fingers subdomain (cf. Figure 1), the helix undergoes an orientational change.[32] By changing the orientation of the O-helix, *taq* pol makes a transition from an "open" to a "closed" state. This causes the dNTP to get closer to the DNA and orient in the appropriate way. The polymerization reaction takes place in this closed state.[32] Three acidic residues (Asp610, Asp785, and Glu786) in the palm subdomain form the active site, and catalyze the addition of the nucleoside to the DNA.[31] The fingers subdomain then repositions back to the open state, and the nucleoside addition process is repeated until either the DNA copying is completed or until the DNA unbinds from the protein.

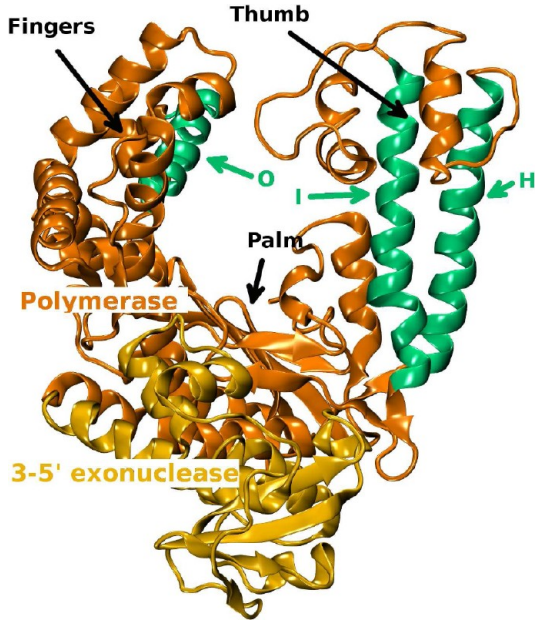

Figure 1. Klentaq fragment of *taq* DNA polymerase has 3′-5′ exonuclease (yellow) and polymerase (orange) domains. The 5′ nuclease domain has been cleaved from the protein and is not shown here. The polymerase domain catalyzes the polymerization reaction. The O-helix in the fingers subdomain and the I- and H-helices in the thumb subdomain are highlighted in green.

In view of biomedical applications, it is interesting to note that all DNA polymerases (including *taq* pol and HIV RT) have unifying features related to their functioning.[33] These include a large conformational change in the fingers subdomain following the DNA substrate binding, and conserved acidic residues located in the palm subdomain, which are in contact with added nucleotides in the DNA synthesis. It is possible that understanding the interactions leading to PCR inhibition would lead to novel insight regarding the effects of fullerene derivatives on the functioning of DNA polymerases and, consequently, replication of genetic material in living systems upon nanomaterial administration or exposure. However, at present, the exact mechanisms of *taq* pol inhibition by fullerene derivatives remain unknown.

Computer simulations have been used to study atomic-scale interactions of fullerenes and their derivatives with various proteins.[23,34−38] An overarching theme of such investigations is to elucidate the structure−function relations of the biological effects of fullerenes. In this work, we have used a combination of docking and molecular dynamics (MD) simulations to study the possible inhibition mechanisms of *taq* pol by two water-soluble fullerene derivatives: the fullerenol $C_{60}(OH)_{20}$ (FUOH) and C_{60} trimalonic acid (TMA).[39] In order to save computational time, only the Klentaq fragment of the protein was used in the simulations.

Docking calculations were first used to assess possible binding sites of the FUOH and TMA, and the related free energy changes. The docked configurations were then used as input for atomistic MD simulations, in which possible changes in the structure and dynamics of *taq* pol upon fullerene derivative binding were studied. Our simulations provide evidence for a noncompetitive or mixed inhibition mechanism, in which binding of fullerene derivatives causes tertiary structure changes to the protein that would affect protein−DNA binding. This mechanism agrees with the available experimental data on *taq* pol inhibition by water-soluble fullerene derivatives.

COMPUTATIONAL METHODS

Docking Calculations. In order to find the most likely binding sites of fullerene derivatives to the Klentaq fragment of *taq* pol, a molecular docking approach[40] was used. FUOH and TMA were docked onto the open (DNA-unbound) and closed (DNA-bound) structures of the protein. The structures of the Klentaq fragment were obtained from the Protein Data Bank (PDB IDs: 1TAQ for the open and 3KTQ for the closed structure).[28,32] Calculations featuring the closed structure included a bound DNA molecule at the active site of the protein (as included in the PDB structure file). The 5′ nuclease domain (residues 1−290) was not present in the 3KTQ structure, and it was removed from the 1TAQ structure. The docking calculations were carried out using the AutoDock docking software, version 4.2,[41] with its default force field parameters.[42] A Lamarckian genetic algorithm[43] was used for sampling molecular conformations, with the number of evaluations set to 2.5×10^7. The protein was considered rigid. The C−C bonds of the C_{60} core of the fullerene derivatives were made nonrotatable, while all other bonds were made flexible.

A hundred independent docking simulations, each with 10 trials, were carried out for each system setup, making a total of 1000 docked configurations of each fullerene derivative-protein structure combination. For each set of docking calculations, the root-mean-square deviations (rmsd's) between the docked configurations were then calculated and those within 0.8 nm were grouped together. Each such group was interpreted to correspond to a binding site of the fullerene derivative, and

dx.doi.org/10.1021/jp3046577 | J. Phys. Chem. B 2012, 116, 10676−10683

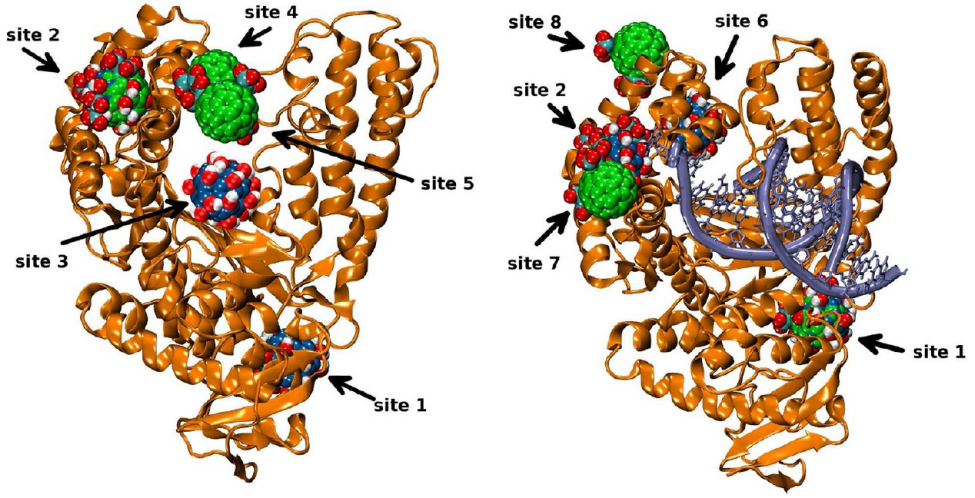

Figure 2. Major binding sites of FUOH (blue C_{60} core) and TMA (green) on *taq* polymerase in the open (left) and closed (right) states, as predicted by the docking calculations. The bound DNA molecule in the case of the closed state is shown in light blue.

different conformations within a group then corresponded to different modes of binding at the same site. It should be noted that our choice for the rmsd cutoff value for grouping the docked configurations was noticeably larger than the typical values of 0.05−0.2 nm used in small ligand-protein docking calculations. This choice was motivated by the spherical symmetry of the fullerene derivatives: rotations around the molecule center of mass will result in large rmsd values for atom positions, although the mode of binding of the fullerene derivative might not change.

The importance of the docking sites was decided according to the following criteria: (a) the binding energy of the fullerene derivative, (b) the number of times the molecule was bound at the site, and (c) the significance of the binding site for the functioning of *taq* pol. The most important docked configurations were chosen for further study in MD simulations.

MD Simulations. The MD simulations were performed using the GROMACS software package,[44] version 4.0.4. The OPLS-AA force field[45] was used for *taq* pol and TIP4P[46] for water. The fullerene derivative models were based on the Lennard-Jones parameters of Girifalco,[47] which have been optimized to reproduce the crystal structure and heat of sublimation of C_{60}. These parameters were recently validated for use with the OPLS force field.[48] All the bonded interaction parameters and Lennard-Jones parameters of functional groups for FUOH and TMA were adapted from the OPLS-AA force field. The partial charges for the FUOH hydroxyl groups were adapted from the OPLS-AA force field, with slight modifications in order to preserve charge neutrality of the molecule. The TMA functional group partial charges were determined by fitting the point charges to a quantum-mechanically determined electrostatic potential, as is commonly done with the OPLS-AA force field. In this study, we only considered the case of the fully ionized form of TMA with a net charge of $-6e$. Further information on the fullerene derivative model parametrizations and GROMACS topology files for FUOH and TMA are provided in the Supporting Information of this article.

Each protein−fullerene derivative complex was placed in a simulation box whose edges were at least 0.9 nm away from the solutes, and then solvated with TIP4P water molecules. In the case of the closed protein structure, the bound DNA molecule was excluded from the MD simulations due to the lack of an optimal parametrization of nucleic acids for the OPLS-AA force field. Na^+ ions were added to charge-neutralize each system (1TAQ and 3KTQ have net charges of $-6e$ and $-7e$, respectively, FUOH is charge neutral, and TMA has a net charge of $-6e$). The system was energy-minimized between each of these steps using the steepest descent algorithm implemented in GROMACS. For equilibrating the system, a 50 ps *NVT* simulation, followed by a 100 ps *NpT* simulation were carried out. In these relaxation simulations, the positions of heavy atoms of *taq* pol and the fullerene derivatives were restrained with a harmonic potential. The system temperature was maintained at 298 K (or 333 K) with the stochastic velocity rescaling algorithm by Bussi et al.,[49] with a coupling time constant of τ_T = 0.1 ps. The protein and all nonprotein molecules were separately coupled to their own thermostats. The system pressure was maintained isotropically at 1 bar with the weak coupling algorithm by Berendsen et al.[50] using a time constant of τ_p = 1.0 ps.

The system relaxation was followed by 50 − 200 ns unrestrained *NpT* sampling simulations. The constant pressure and temperature conditions in these simulations were maintained by a Parrinello−Rahman barostat[51] (τ_p = 2.0 ps) and a velocity rescaling thermostat (τ_T = 0.1 ps). In all the simulations, Lennard-Jones interactions were cut off at 1.4 nm without any switch or shift functions, and long-range corrections were applied to both pressure and energy. Electrostatic interactions were handled using the smooth PME method[52,53] with a real-space cutoff of 0.9 nm. The simulation time step was 2 fs. All bonds in the simulated molecules were constrained to their reference values with LINCS.[54]

Before running the actual protein-FUOH/TMA complex simulation series, the stability of the Klentaq fragment with the OPLS-AA force field was ascertained. Overall, the secondary structure was well preserved. The only noticeable exception to this was the tip of the thumb subdomain, which was very flexible. This part of the protein undergoes a conformational change when DNA binds to the protein.[32] For further information on the protein-only simulations, please refer to the Supporting Information.

RESULTS

Docking Calculations. The most important binding sites of fullerene derivatives with the open and closed states of *taq* pol are shown in Figure 2. The respective binding energies and frequencies (expressed as the percentage of population over all docked configurations) are summarized in Table 1. The binding energies of TMA were overall higher than those of FUOH, most likely due to the electrostatic interaction of the fully ionized malonic acid functional groups with the protein residues. Site **2**, located in the fingers subdomain, was a major binding site for all FUOH/TMA-protein structure combinations. The binding energies at this site were 19.7 and 23.7 kJ/mol for FUOH and 38.8 and 31.3 kJ/mol for TMA in the case of the open and closed structures, respectively. Site **1**, situated in the posterior side of the protein (with respect to the DNA binding site), at the interface between exonuclease and polymerase domains, was also a major binding site in all cases except for TMA and the open structure of *taq* pol. Both of these binding sites were further studied with MD simulations.

Site **3** was an important binding site only in the case of FUOH and the open protein structure (binding energy 16.4 kJ/mol). This binding site is not accessible to fullerene derivatives when DNA is bound to the protein. However, as the site is close to the polymerase active site, it was also included in the MD simulations.

Sites **4** and **5**, located between the fingers and thumb subdomains (see Figure 2), had significant binding energies (48.1 and 35.9 kJ/mol, respectively) for TMA docking with the open structure. These sites also corresponded to about 75% of all docked configurations in that case. However, both sites are located in highly flexible loop regions of the thumb subdomain; therefore, we expect these sites not to be persistent binding sites. For this reason, we did not start MD simulations from structures with FUOH or TMA docked to these two sites. It should be noted that similar modes of binding were observed in the MD simulations in which fullerene derivatives were placed in random positions around the protein (see below).

A possible mechanism of polymerase inhibition could involve binding at sites **6** and **8**, found in the docking calculations with the closed protein structure: the bound fullerene derivatives could prevent the transition from the closed to the open state of *taq* pol. MD simulations with FUOH bound at site **6** were carried out to explore this possibility for polymerase inhibition. Finally, site **7** was excluded from MD simulations due to the lack of a plausible mechanism of inhibition.

MD Simulations. MD simulations allowed us to study how fullerene derivative binding affects the structure and dynamics of *taq* pol. To this end, two types of protein-FUOH/TMA complex simulations were carried out. In the first set, a single fullerene derivative molecule was placed at a binding site predicted by the docking calculations. For each binding site studied, one initial fullerene derivative-protein configuration was used, and the atoms were assigned random velocities according to the respective temperature. The second set featured simulations with 10 molecules of the same type. In each independent simulation, the fullerene derivatives were placed by hand at random locations around the protein using the molecular visualization software VMD.[55] All these simulations were performed on the open structure of the protein at 298 K. Since PCR involves repeated heating and cooling of the reaction solution, some simulations were repeated at 333 K in order to check the effect of temperature. Finally, simulations with FUOH or TMA placed at site **2** and FUOH placed at site **6** were performed with the closed structure. The protein−fullerene derivative MD simulation series, along with protein-only reference simulations (designated with the code APO), are summarized in Table 2. Unless stated otherwise, the results discussed below refer to simulations in the case of the open structure of *taq* pol at 298 K. Due to the large number of simulations performed, in the following we will refer to each simulation using the code listed in Table 2.

Table 1. Major Binding Sites of FUOH and TMA on the Open and Closed Structures of *Taq* Pol, with Their Binding Energies E_b and Population (pop)[a]

site	E_b(kJ/mol)	pop (%)	open/closed state	MD
FUOH, open state				
1	24.0	11.0	both	•
2	19.7	55.8	both	•
3	16.4	7.6	both	•
FUOH, closed state				
1	21.1	10.5	both	
2	23.7	58.0	both	•
6	5.8	3.6	closed	•
TMA, open state				
2	38.8	8.0	both	•
4	48.1	38.3	open	
5	35.9	37.2	open	
TMA, closed state				
1	27.5	9.6	both	
2	31.3	43.2	both	•
7	27.1	29.3	both	
8	27.0	7.1	closed	

[a]The table also shows whether the binding site in question was found for the open, closed, or both states of the protein, and whether the fullerene derivative binding site pair was included in the MD simulation studies (•). The binding sites are shown in Figure 2.

Table 2. Summary of the Systems Studied in the MD Simulations[a]

code	system	#	time (ns)
Open State (1TAQ), T = 298 K			
APO	protein only	4	100, 3 × 50
S1F	1 FUOH at site 1	3	3 × 50
S2F	1 FUOH at site 2	3	3 × 50
S3F	1 FUOH at site 3	3	3 × 50
S2T	1 TMA at site 2	2	100, 50
R10F	10 FUOH randomly placed	6	2 × 100, 4 × 50
R10T	10 TMA randomly placed	6	2 × 100, 4 × 50
Open State (1TAQ), T = 333 K			
APO*	protein only	3	100, 2 × 50
R10F*	10 FUOH randomly placed	3	100, 2 × 50
R10T*	10 TMA randomly placed	3	100, 2 × 50
Closed State (3KTQ), T = 298 K			
APO[c]	protein only	2	2 × 200
S2F[c]	1 FUOH at site 2	2	100, 50
S6F[c]	1 FUOH at site 6	2	100, 50
S2T[c]	1 TMA at site 2	2	100, 50

[a]The table lists the codes assigned to each specific simulation set-up, explanation of the set-up, number of independent simulations, and simulation time of each independent run.

dx.doi.org/10.1021/jp3046577 | J. Phys. Chem. B 2012, 116, 10676−10683

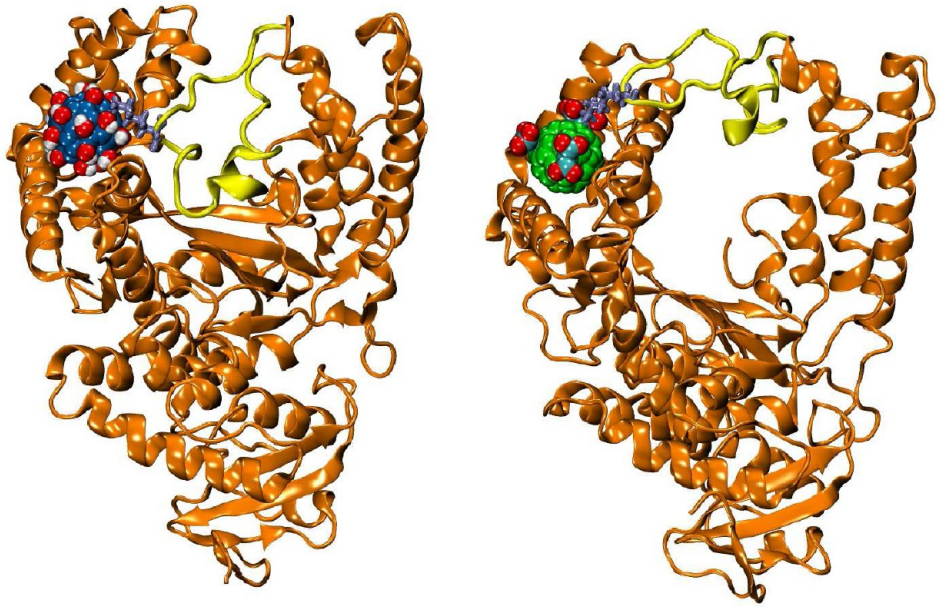

Figure 3. Movement of the tip of the thumb subdomain (yellow) toward the fingers subdomain was seen when fullerene derivatives were bound at site **2**. The residues Lys505 and Lys508, which strongly interact with the bound fullerene derivatives, are shown in stick representation as light blue.

Fullerene derivatives placed at docking sites predominantly remained bound at the same sites. This indicates that the sites predicted by docking were indeed favorable binding sites for FUOH and TMA. The only exception to these results was one of the S2F simulations (starting from a structure with a FUOH molecule docked at site **2**). In this case, after 3 ns of simulation time, the FUOH molecule moved a distance of approximately 1 nm on the palm subdomain from its initial position and stayed in that location for the remainder of the simulation. This new location, denoted in the following as site **3A**, was not predicted in the docking calculations. This was probably due to the inflexibility of the protein structure in the docking calculations. In MD simulations, the residues could readjust themselves to accommodate the fullerene derivatives, thus providing a new binding site.

As explained previously, the docking calculations predicted that the binding was in general stronger for TMA compared to FUOH. This indeed was reflected in the MD interaction energies. Even though there was no significant difference in the Lennard-Jones interactions of protein with FUOH and TMA, the electrostatic interactions were much stronger with TMA. At site **2**, for instance, the average electrostatic interaction energy with the protein was −503 kJ/mol for TMA, whereas it was only −83 kJ/mol for FUOH. This is because the anionic TMA interacted strongly with positively charged side chains of residues, such as arginine and lysine. FUOH, on the other hand, interacted with both charged and uncharged polar residues, but the (dipolar) interactions were not as strong as in the case of TMA. At site **2**, residues Arg704, Arg715, Lys738, and Arg746 interacted with TMA during almost the whole simulation time, whereas only Arg704 and Arg715 interacted with FUOH for a comparably long time.

In two S2F and one of the S2T simulations (fullerene derivatives at site **2**), the tip of the thumb subdomain moved toward the binding site and made several contacts. In particular, the thumb residues Lys505 and Lys508 made contact with the fullerene derivatives bound at the site (see Figure 3). The thumb-to-fingers binding was strong enough to prevent the thumb from retracting back to the initial unbound conformation during the remainder of the simulations.

In some of the R10F and R10T simulations, a significant change in the tertiary structure of the protein was observed. In two of the R10F simulations, FUOH binding at the two thumb helices (H-helix, residues 453−477, and I-helix, residues 527−552) caused the helices to bend (see Figure 4). This kind of bending was not observed in any of the APO, SxF, or SxT simulations, where fullerene derivatives did not bind to the helices in question. In the R10T simulations, the tip of the thumb subdomain moved toward the fingers subdomain. In these simulations, the same TMA molecule was bound to the fingers subdomain and the tip of the thumb subdomain, and prevented the thumb domain from moving back.

To quantify the thumb-to-fingers movement, we defined two groups of residues: one in the thumb subdomain (residues 496−510), and the other in the fingers subdomain (residues 673−690 and 732−742). The distance between the centers of mass of these two groups was then calculated as a function of time for all the APO, R10F, and R10T simulations (see Figure 5). The average value of this distance during the last 10 ns of the simulations was 2.6 ± 0.3 nm for APO, 2.2 ± 0.4 nm for R10F, and 1.5 ± 0.2 nm for R10T simulations (the errors here refer to the standard deviation of values averaged over independent runs of the same system). In one R10F simulation none of the FUOH molecules were bound near the tip of the thumb or fingers, and consequently no thumb-to-fingers movement was seen. If this particular simulation was excluded from the analysis, the average distance between the centers of masses of the two residue groups was reduced to 2.0 ± 0.2 nm.

In comparison to simulations at 298 K, simulations at 333 K showed no significant change in the structure of protein or binding of nanoparticles. In order to ascertain that this result was not an artifact of the finite simulation times used, the structural convergence of the trajectories was determined using the decorr_time tool included in the LOOS analysis package.[56] The decorrelation times for all the simulations at 333 K, both with and without the fullerene derivatives, were 5−8 ns (i.e.,

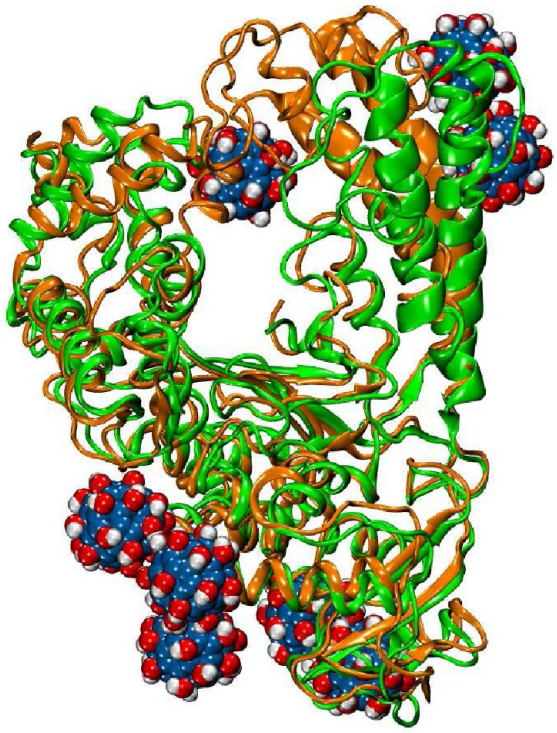

Figure 4. Bending of helices caused by FUOH binding seen in a simulation in which FUOH molecules were initially placed randomly around the protein (R10F simulation). The crystal structure of the protein is shown in green and the structure at the end of the 50 ns R10F simulation is shown in orange.

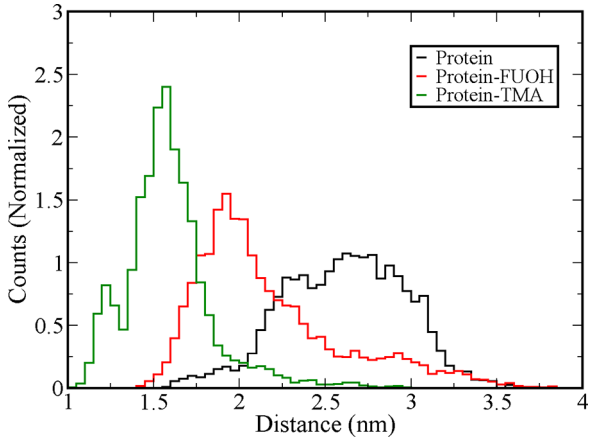

Figure 5. Distance between centers of mass of two groups of residues in the fingers and thumb subdomains (see text). The residue group separations are clearly smaller for protein−fullerene derivative complex simulations.

roughly an order of magnitude shorter than the simulation times). This ensured that the simulation lengths were adequate. The results of the decorrelation time analysis are included in the Supporting Information.

As in the simulations starting from the open structure (T = 298 K), in the simulations starting from the closed structure, FUOH and TMA remained at their binding sites during the entire simulation. Our initial assumption was that the isolated protein would open in the absence of the nucleic acid. However, neither one of the APO simulations showed a transition from closed to open structure. It is possible that the closed state is a local free energy minimum even in the absence of nucleic acids. In that case, much longer simulations would be required for reliable quantification the opening process. This, however, was beyond the scope of the present study.

DISCUSSION

The docking and MD simulations strongly indicate that FUOH and TMA do not interact with the active site of *taq* pol. The active site is situated in the cleft of the palm subdomain and although site **3** is in its vicinity, the fullerene derivatives are too large to fit there (based on steric arguments). It thus seems unlikely that FUOH or TMA inhibit PCR by direct binding at the active site of *taq* pol.

At site **3** (in the palm subdomain), FUOH made contact with a large number of protein residues, forming hydrogen bonds with residues Ala570, Thr571, Gln582, Asn583, Asn750, and Gln754. Further, when FUOH was at site **3A**, it formed hydrogen bonds with the residues Thr385, Ala568, Cys576, Cys577, Asp578, and Asn580. Interestingly, during the polymerization reaction, a DNA molecule binds to the enzyme making contact with many of the same residues, including Ala568, Cys577 (Ser577), Asn580, Asn583, Asn750, and Gln754.[31] This means that FUOH bound at site **3** or **3A** competes with DNA for many of the same hydrogen bonding partners. This could provide a mechanism of direct inhibition for FUOH, as the polymerase activity is not possible without DNA binding. However, TMA did not bind at site **3** in any of our simulations, and thus its inhibiting effect cannot be explained by this mechanism. Moreover, inhibition due to binding of FUOH at site **3** would imply a competitive mechanism. Consequently, the PCR inhibition would be reversed by increasing the concentration of the DNA for a given concentration of FUOH. However, the experiments by Meng et al. showed that the inhibition could not be reversed by the addition of DNA at a fixed FUOH or TMA concentration.[26] Reversal of the inhibition upon an increase in *taq* pol concentration was observed instead. In view of these data, we conclude that, although FUOH binding close to the active site can contribute to the polymerase inhibition, it cannot be the only mechanism. Additionally, this mechanism is probably not available in the case of TMA.

In the R10F and R10T simulations, the tertiary structure of *taq* pol was significantly altered in different ways by fullerene derivative binding. The FUOH molecules bent two α helices of the thumb subdomain. One of these two helices, the I-helix, makes a number of contacts with DNA.[31] Similarly, TMA (and also FUOH but to a lesser extent) caused the binding of the tip of the thumb subdomain with the fingers subdomain. Similar thumb-to-fingers binding was also seen when either FUOH or TMA was located at site **2** in the fingers subdomain. The tip of the thumb subdomain undergoes a transition upon DNA binding and also makes a number of contacts with the bound DNA. These tertiary structure changes due to fullerene derivative binding can reduce or prevent DNA binding to the protein and hence decrease or suppress polymerase activity. Inhibition due to tertiary structure changes is not competitive and hence it cannot be reversed by increasing the DNA concentration for a given fullerene derivative concentration. On the other hand, by increasing the polymerase concentration, the activity should be regained as it also increases the possibility of the DNA interacting with a polymerase without a bound fullerene derivative. Our findings thus suggest a noncompeti-

dx.doi.org/10.1021/jp3046577 | J. Phys. Chem. B 2012, 116, 10676−10683

tive/mixed inhibition mechanism, common to both FUOH and TMA, in agreement the experimental results.[26,27]

One way to experimentally verify our computational findings would be by point mutation studies. For example, one could devise point mutations that preserve protein structure and activity and reduce inhibition by fullerene derivatives. According to our simulations, binding of fullerene derivatives is not very specific, with the exception of a few favorable binding sites. Some binding sites (e.g., the tip of the thumb and fingers subdomains) are also involved in DNA binding. Most residues in these regions are conserved among proteins in the same family, probably due to their importance for DNA binding. Point mutations in those regions would probably lead to loss of enzyme function. It is interesting to note that most of the fullerene derivative binding residues at site **2** are not involved in DNA binding, and some are not conserved across different species. Furthermore, FUOH and TMA mainly interact with different residues at that site: FUOH binds predominantly to residues Glu708, Glu742, Glu745, and Arg746, while TMA binds only to Arg746. Glu745 is somewhat conserved, Arg746 is absolutely conserved, but Glu708 and Glu742 are not conserved at all. If fullerene derivative binding at site **2** inhibits enzyme activity, as suggested by our simulations, it should be possible to design point mutations that reduce inhibition (provided that the structure of the protein remains intact). Careful choice of point mutations could result in selective inhibition by only one of the fullerene derivatives, validating the simulation results.

CONCLUSIONS

In this work we studied the inhibition mechanism of *taq* DNA polymerase by fullerene derivatives using molecular docking and MD simulations. The important binding sites of fullerene derivatives on *taq* pol were identified using docking simulations. MD simulations of the docked structures showed that these sites are indeed stable binding sites. Fullerene derivative binding at site **2** caused a conformational change in the protein, leading to a close contact between the thumb and the finger subdomain. MD simulations with random distributions of FUOH or TMA around the protein were also performed. In these simulations, thumb-to-fingers contact and bending of two helices in the thumb subdomain were observed. Our study suggests that these changes in the tertiary structure can affect *taq* pol-DNA binding, and hence can be responsible for the inhibition of the enzyme activity observed in experiments.

ASSOCIATED CONTENT

Supporting Information

Analysis of the protein-only (APO) simulations and *taq* pol conformational decorrelation times at T = 333 K (protein-only, and with bound fullerene derivatives), as well as structure (PDB) and GROMACS topology files for FUOH and TMA used in this study. This material is available free of charge via the Internet at http://pubs.acs.org/.

AUTHOR INFORMATION

Corresponding Author

*E-mail: emppu.salonen@aalto.fi.

Notes

The authors declare no competing financial interest.

ACKNOWLEDGMENTS

We thank Professor Pu-Chun Ke (Clemson University, Clemson, SC, USA) for his insightful comments on the manuscript. This work was supported by the Academy of Finland (project no. 127091) and HPC Europa2 (Grant No. 228398). Computational resources provided by CSC - The Finnish IT Center for Science and CINES are gratefully acknowledged. P.N.G. is thankful to Agnel Praveen Joseph for his help in using the ConSurf server.

REFERENCES

(1) Jensen, A. W.; Wilson, S. R.; Schuster, D. I. *Bioorg. Med. Chem.* **1996**, *4*, 767−779.
(2) Da Ros, T.; Prato, M. *Chem. Commun.* **1999**, 663−669.
(3) Bosi, S.; Ros, T. D.; Spalluto, G.; Prato, M. *Eur. J. Med. Chem.* **2003**, *38*, 913−923.
(4) Bakry, R.; Vallant, R. M.; Najam-ul-Haq, M.; Rainer, M.; Szabo, Z.; Huck, C. W.; Bonn, G. K. *Int. J. Nanomed.* **2007**, *2*, 639−649.
(5) Partha, R.; Conyers, J. L. *Int. J. Nanomed.* **2009**, *4*, 261−275.
(6) Shinohara, H. *Rep. Prog. Phys.* **2000**, *63*, 843−892.
(7) Arbogast, J. W.; Darmanyan, A. P.; Foote, C. S.; Rubin, Y.; Diederich, F. N.; Alvarez, M. M.; Anz, S. J.; Whetten, R. L. *J. Phys. Chem.* **1991**, *95*, 11−12.
(8) Shen, L.; Ji, H.-F.; Zhang, H.-Y. *Photochem. Photobiol.* **2006**, *82*, 798−800.
(9) Hirsch, A. *J. Phys. Chem. Solids* **1997**, *58*, 1729−1740.
(10) Taylor, R., Ed. *The Chemistry of Fullerenes*; World Scientific Publishing Co. Ltd.: Singapore, 2003.
(11) Martín, N. *Chem. Commun.* **2006**, 2093−2104.
(12) Nakamura, E.; Isobe, H. *Acc. Chem. Res.* **2003**, *36*, 807−815.
(13) Zhang, W.; Sprafke, J. K.; Ma, M.; Tsui, E. Y.; Sydlik, S. A.; Rutledge, G. C.; Swager, T. M. *J. Am. Chem. Soc.* **2009**, *131*, 8446−8454.
(14) Mikawa, M.; Kato, H.; Okumura, M.; Narazaki, M.; Kanazawa, Y.; Miwa, N.; Shinohara, H. *Bioconjugate Chem.* **2001**, *12*, 510−514.
(15) Kato, H.; Kanazawa, Y.; Okumura, M.; Taninaka, A.; Yokawa, T.; Shinohara, H. *J. Am. Chem. Soc.* **2003**, *125*, 4391−4397.
(16) Nakamura, E.; Isobe, H.; Tomita, N.; Sawamura, M.; Jinno, S.; Okayama, H. *Angew. Chem., Int. Ed.* **2000**, *39*, 4254−4257.
(17) Maeda-Mamiya, R.; Noiri, E.; Isobe, H.; Nakanishi, W.; Okamoto, K.; Doi, K.; Sugaya, T.; Izumi, T.; Homma, T.; Nakamura, E. *Proc. Natl. Acad. Sci. U.S.A.* **2010**, *107*, 5339−5344.
(18) Chaudhuri, P.; Paraskar, A.; Soni, S.; Mashelkar, R. A.; Sengupta, S. *ACS Nano* **2009**, *3*, 2505−2514.
(19) Markovic, Z.; Trajkovic, V. *Biomaterials* **2008**, *29*, 3561−3573.
(20) Tokuyama, H.; Yamago, S.; Nakamura, E. *J. Am. Chem. Soc.* **1993**, *115*, 7918−7919.
(21) Ikeda, A.; Sato, T.; Kitamura, K.; Nishiguchi, K.; Sasaki, Y.; Kikuchi, J.; Ogawa, T.; Yogo, K.; Takeya, T. *Org. Biomol. Chem.* **2005**, *3*, 2907−2909.
(22) Wang, D.; Sun, L.; Liu, W.; Chang, W.; Gao, X.; Wang, Z. *Environ. Sci. Technol.* **2009**, *43*, 5825−5829.
(23) Friedman, S. H.; DeCamp, D. L.; Sijbesma, R. P.; Srdanov, G.; Wudl, F.; Kenyon, G. L. *J. Am. Chem. Soc.* **1993**, *115*, 6506−6509.
(24) Mashino, T.; Shimotohno, K.; Ikegami, N.; Nishikawa, D.; Okuda, K.; Takahashi, K.; Nakamura, S.; Mochizuki, M. *Bioorg. Med. Chem. Lett.* **2005**, *15*, 1107−1109.
(25) Pabla, S. S.; Pabla, S. S. *Resonance* **2008**, *13*, 369−3777.
(26) Meng, X.; Li, B.; Chen, Z.; Yao, L.; Zhao, D.; Yang, X.; He, M.; Yu, Q. *J. Enzyme Inhib. Med. Chem.* **2007**, *22*, 293−296.
(27) Shang, J.; Ratnikova, T. A.; Anttalainen, S.; Salonen, E.; Ke, P. C.; Knap, H. T. *Nanotechnology* **2009**, *20*, 415101.
(28) Kim, Y.; Eom, S. H.; Wang, J.; Lee, D.-S.; Suh, S. W.; Steitz, T. A. *Nature* **1995**, *376*, 612−616.
(29) Steitz, T. A. *J. Biol. Chem.* **1999**, *274*, 17395−17398.
(30) Barnes, W. M. *Gene* **1992**, *112*, 29−35.
(31) Eom, S. H.; Wang, J.; Steitz, T. A. *Nature* **1996**, *382*, 278−281.

(32) Li, Y.; Korolev, S.; Waksman, G. *EMBO J.* **1998**, *17*, 7514−7525.
(33) Doublié, S.; Sawaya, M. R.; Ellenberger, T. *Structure* **1999**, *7*, R31−R35.
(34) Noon, W. H.; Kong, Y.; Ma, J. *Proc. Natl. Acad. Sci. U.S.A.* **2002**, *99*, 6466−6470.
(35) Benyamini, H.; Shulman-Peleg, A.; Wolfson, H. J.; Belgorodsky, B.; Fadeev, L.; Gozin, M. *Bioconjugate Chem.* **2006**, *17*, 378−386.
(36) Durdagi, S.; Supuran, C. T.; Strom, T. A.; Doostdar, N.; Kumar, M. K.; Barron, A. R.; Mavromoustakos, T.; Papadopoulos, M. G. *J. Chem. Inf. Model.* **2009**, *49*, 1139−1143.
(37) Calvaresi, M.; Zerbetto, F. *ACS Nano* **2010**, *4*, 2283−2299.
(38) Kraszewski, S.; Tarek, M.; Treptow, W.; Ramseyer, C. *ACS Nano* **2010**, *4*, 4158−4164.
(39) Lamparth, I.; Hirsch, A. *J. Chem. Soc., Chem. Commun.* **1994**, 1727−1728.
(40) Lengauer, T.; Rarey, M. *Curr. Opin. Struct. Biol.* **1996**, *6*, 402−406.
(41) Morris, G. M.; Huey, R.; Lindstrom, W.; Sanner, M. F.; Belew, R. K.; Goodsell, D. S.; Olson, A. J. *J. Comput. Chem.* **2009**, *30*, 2785−2791.
(42) Huey, R.; Morris, G. M.; Olson, A. J.; Goodsell, D. S. *J. Comput. Chem.* **2007**, *28*, 1145−1152.
(43) Morris, G. M.; Goodsell, D. S.; Halliday, R. S.; Huey, R.; Hart, W. E.; Belew, R. K.; Olson, A. J. *J. Comput. Chem.* **1998**, *19*, 1639−1662.
(44) Hess, B.; Kutzner, C.; van der Spoel, D.; Lindahl, E. *J. Chem. Theory Comput.* **2008**, *4*, 435−447.
(45) Jorgensen, W. L.; Maxwell, D. S.; Tirado-Rives, J. *J. Am. Chem. Soc.* **1996**, *118*, 11225−11236.
(46) Kaminski, G. A.; Friesner, R. A.; Tirado-Rives, J.; Jorgensen, W. L. *J. Phys. Chem. B* **2001**, *105*, 6474−6487.
(47) Girifalco, L. A. *J. Phys. Chem.* **1992**, *96*, 858−861.
(48) Monticelli, L. *J. Chem. Theory Comput.* **2012**, *8*, 1370−1378.
(49) Bussi, G.; Donadio, D.; Parrinello, M. *J. Chem. Phys.* **2007**, *126*, 014101.
(50) Berendsen, H. J. C.; Postma, J. P. M.; van Gunsteren, W. F.; DiNola, A.; Haak, J. R. *J. Chem. Phys.* **1984**, *81*, 3684−3690.
(51) Parrinello, M.; Rahman, A. *J. Appl. Phys.* **1981**, *52*, 7182−7190.
(52) Darden, T.; York, D.; Pedersen, L. *J. Chem. Phys.* **1993**, *98*, 10089−10092.
(53) Essmann, U.; Perera, L.; Berkowitz, M. L.; Darden, T.; Lee, H.; Pedersen, L. G. *J. Chem. Phys.* **1995**, *103*, 8577−8593.
(54) Hess, B.; Bekker, H.; Berendsen, H. J. C.; Fraaije, J. G. E. M. *J. Comput. Chem.* **1997**, *18*, 1463−1472.
(55) Humphrey, W.; Dalke, A.; Schulten, K. *J. Mol. Graphics* **1996**, *14*, 33−38.
(56) Romo, T. D.; Grossfield, A. *EMBC 2009, 31st Annual International Conference of the IEEE Engineering in Medicine and Biology Society*; IEEE: Piscataway, NJ, 2009; pp 2332−2335, doi: 10.1109/IEMBS.2009.5335065.